IPEM Institute of Physics and Engineering in Medicine

A scintillator-based range telescope for particle therapy

A scintillator-based range telescope for particle therapy

Laurent Kelleter[1], Raffaella Radogna[1], Lennart Volz[2,3], Derek Attree[1], Anastasia Basharina-Freshville[1], Joao Seco[2,3], Ruben Saakyan[1] and Simon Jolly[1]

[1]Dept. Physics and Astronomy, University College London, Gower Street, WC1E 6BT London, UK

[2] Department of Biomedical Physics in Radiation Oncology, German Cancer Research Center (DKFZ), Heidelberg, GER

[3] Department of Physics and Astronomy, Heidelberg University, Heidelberg, GER

E-mail: laurent.kelleter@ucl.ac.uk

Abstract.

The commissioning and operation of a particle therapy centre requires an extensive set of detectors for measuring various parameters of the treatment beam. Among the key devices are detectors for beam range quality assurance. In this work, a novel range telescope based on plastic scintillator and read out by a large-scale CMOS sensor is presented. The detector is made of a stack of 49 plastic scintillator sheets with a thickness of 2–3 mm and an active area of 100×100 mm^2, resulting in a total physical stack thickness of 124.2 mm. This compact design avoids optical artefacts that are common in other scintillation detectors. The range of a proton beam is reconstructed using a novel Bragg curve model that incorporates scintillator quenching effects. Measurements to characterise the performance of the detector were carried out at the Heidelberger Ionenstrahl-Therapiezentrum (HIT, Heidelberg, GER) and the Clatterbridge Cancer Centre (CCC, Bebington, UK). The maximum difference between the measured range and the reference range was found to be 0.41 mm at a proton beam range of 310 mm and was dominated by detector alignment uncertainties. With the new detector prototype, the water-equivalent thickness of PMMA degrader blocks has been reconstructed within ± 0.1 mm. An evaluation of the radiation hardness proves that the range reconstruction algorithm is robust following the deposition of 6,300 Gy peak dose into the detector. Furthermore, small variations in the beam spot size and transverse beam position are shown to have a negligible effect on the range reconstruction accuracy. The potential for range measurements of ion beams is also investigated.

A scintillator-based range telescope for particle therapy   2

1. Introduction

Particle therapy is a form of highly targeted radiation therapy that is used to treat certain types of cancer. It has seen a boom in the past two decades with more than ninety centres being operational worldwide as of 2019 — most of which are proton therapy centres — and more facilities being in the construction or planning phase [1]. The key advantage of particle therapy, relative to conventional photon radiotherapy, is the characteristic dose distribution through the patient with a low entrance dose that increases to a maximum — the Bragg peak — beyond which very little dose is deposited. This enables the tumour to be targeted with greater precision than in photon radiotherapy. The healthy tissue surrounding the tumour can therefore be spared more effectively [2]. Due to the large dose gradient it is essential for a safe and effective treatment to know the exact location of the Bragg peak. A significant amount of time is therefore dedicated to measuring percent depth-dose curves (PDD) that characterise the longitudinal dose distribution of the particle beam — and therefore the precise depth of the Bragg peak — during both the commissioning of the centre [3] and regular quality assurance during clinical operation [4, 5, 6].

The gold standard for measuring reference PDD curves are ionisation chambers that are immersed in a water tank in order to scan the pencil beam at different depths and transverse positions [7]. Such water phantoms are used for dosimetry as well as for beam range measurements. However, scanning the PDD curve by moving the ionisation chamber along the Bragg curve is time consuming and can take several minutes for a single pencil beam. Many centres therefore use faster detectors for beam range measurements, such as Multi-Layer Ionisation Chambers (MLIC) [5]. However, they suffer from different drawbacks: ionisation chambers are not inherently water-equivalent and need to be sandwiched with suitable absorber material such that the MLIC measures water-equivalent thickness (WET). Also, the finite size of their charge-collecting electrodes complicates the measurement of integrated depth-dose curves [8] which is why commercial MLICs (e.g., from IBA Dosimetry, Schwarzenbruck, Germany) are available with differently sized electrodes for the measurement of either large (IBA Zebra) or small (IBA Giraffe) fields. Furthermore, ionisation chambers exhibit dose-rate effects [9] and need to be cautiously recalibrated when used outside of reference conditions [7]. Finally, the analogue electronics used in the charge collection and measurement can make MLICs fragile and susceptible to damage if not handled carefully.

In the absence of ideal instrumentation for particle beam measurements, alternative detector systems based on scintillating materials have been investigated by several groups in order to complement ionisation chambers [10]. A scintillator is a material that emits light in response to the deposition of energy by ionising radiation. Organic scintillators are composed of a synthetic polymer base such as polystyrene (PS) or polyvinyl toluene (PVT), a primary dopant that converts the UV radiation of the base into visible light and a secondary dopant that acts as a wavelength shifter [11]. The latter ensures that the scintillator is transparent to its own scintillation light. Organic

A scintillator-based range telescope for particle therapy 3

77 scintillators exhibit multiple characteristics that make them interesting for applications
78 in particle therapy detectors such as the low price, fast signal rise time, scalability,
79 dose-rate independence and nearly water-equivalent density [11].

80 Historically, scintillators have been avoided for reference dosimetry in particle
81 therapy because they suffer from radiation damage and exhibit light quenching effects.
82 The light quenching leads to a non-linear dependence between light output and dose
83 deposition for particles with high energy losses (linear energy transfer, LET) such
84 as protons [12]. However, scintillating screens are commonly used for beam spot
85 position [13] and field homogeneity measurements [7]. Moreover, scintillating screens
86 have successfully been employed for Percent Depth-Light curve (PDL) measurements in
87 water phantoms [14, 15]. Fukushima et al. suggested using a block of plastic scintillator
88 and a commercial digital camera for the fast acquisition of PDL curves [16]. This
89 idea was further developed by other groups [17, 18]. Moreover, a detector based on
90 liquid scintillator for fast quasi-3D pencil beam measurements was developed at M.D.
91 Anderson Cancer Center (Houston, Texas, USA) [19, 20, 21]. However, all these devices
92 have in common that they have to correct for optical artefacts that come with the use
93 of a digital camera to record the light output [22]. In addition, complex high-resolution
94 simulations of the LET distribution in the scintillator are necessary in order to correct
95 for quenching effects [23, 24].

96 A novel range telescope based on a stack of thin sheets of plastic scintillator is
97 under development at University College London (UCL, London, UK). The evaluation
98 of a prototype detector is presented in this work. The application of the detector
99 focuses on the range measurement of particle pencil beams, similar to a MLIC. The
100 scintillation light is read out with a large-scale CMOS sensor which is directly coupled
101 to the scintillator stack. This configuration avoids optical artefacts and allows a very
102 compact detector design. The light quenching is not corrected for in the detector itself
103 but is accounted for by utilising a new model of a quenched Bragg curve which was
104 found to reconstruct the proton beam range within ± 0.16 mm [25].

2. Materials and Methods

2.1. Scintillator

107 The range telescope has a segmented design using 49 thin scintillator sheets with a
108 transverse area of 100×100 mm^2 and a thickness between 2 and 3 mm: the schematic
109 design is shown in figure 1(a). The transverse sheet size ensures that the majority of the
110 dose from a conventional therapeutic proton pencil beam is absorbed in the scintillator,
111 whereas the sheet thickness is a compromise between required spatial resolution and
112 mechanical stability.

113 The sheets are composed of a polystyrene-based scintillator (Nuvia a.s., Třebíč,
114 Czech Republic) with a density of 1.03 ± 0.01 g cm^{-3}, a decay constant of 2.5 ns and a
115 light output of 56% of that of anthracene [26]. Each sheet is sprayed with a thin layer
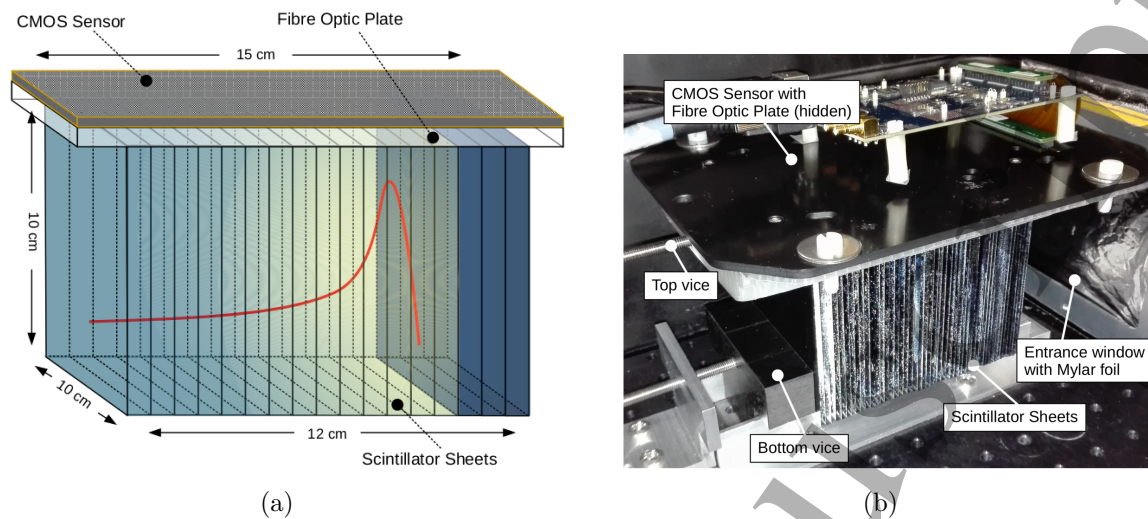
Figure 1. (a) Sketch and (b) photograph of the prototype scintillator-based range telescope with thin scintillator sheets and a CMOS sensor readout.

116 — between 0.01-0.07 mm per sheet — of matt black spray paint (Halfords, Redditch,
117 UK) in order to ensure optical decoupling. Two side orthogonal faces of each sheet
118 were left unpainted to allow the scintillation light to emerge and be simultaneously
119 measured with different devices. The top face was coupled to the CMOS sensor and
120 the light from the second unpainted face was recorded with a DSLR camera. The
121 results of the latter readout device are not shown in this work. The density of the
122 dried paint film provided by the manufacturer is 1.231 g cm^{-3}. The thickness of all
123 painted scintillator sheets was measured individually at room temperature at eight
124 points around the sheet with a micrometer screw gauge. The physical thickness of the
125 full scintillator sheet stack is 124.20 mm, giving an average sheet thickness of 2.53 mm.
126 The average standard deviation of the sheet thickness is 0.02 mm. The uncertainty
127 on the physical thickness of the whole stack due to thermal expansion is calculated
128 to be smaller than ±0.02 mm [27]. The water equivalent thickness of the painted
129 scintillator stack was determined by measuring the range pull-back of a carbon ion
130 beam (270 MeV/u) with a Peakfinder (PKF) water column (PTW, Freiburg, Germany)
131 and found to be 127.27$\pm$0.04 mm. The WET was also measured with a proton and
132 a helium beam and the measured values agreed within the measurement uncertainty
133 (0.04 mm). The displaced air was taken into account in the calculation of the WET.

134 *2.2. CMOS Sensor*

135 A large-scale CMOS image sensor (ISDI, London, UK) is used for the detection of the
136 scintillation light output. The sensor has an active area of 153.6×103.0 mm^2, a pixel
137 size of 0.1×0.1 mm^2 and a resolution of 1536×1030 pixels: each of the 1536 rows has
138 a length of 1030 pixels. The sensor is operated in rolling-shutter mode, i.e. the sensor
139 is read out row by row. Two pixel rows are read out simultaneously. The readout of a

A scintillator-based range telescope for particle therapy   5

140 pixel row pair takes 0.02 ms during which no charge is accumulated (dead time). The
141 frame rate of the sensor is 25 frames per second (fps). This makes the total acquisition
142 time per frame 40 ms of which readout takes 15 ms. The minimum delivery time of a
143 pencil beam is therefore 15 ms.

144 Image frames are transferred via a Camera Link cable to a PIXCI E8 PCI Express
145 (PCIe) x8 Frame Grabber (EPIX Inc., Buffalo Grove, Illinois, USA). The PCIe card is
146 inserted in a PCIe x16 Expansion Chassis (StarTech.com, Lockbourne, Ohio, USA) that
147 is connected to a computer with a Thunderbolt 3 cable. The images are saved using the
148 software XCAP-Lite v3.8 for Windows (EPIX Inc.), which comes with the PCIe card.
149 A maximum of 21 full resolution images can be taken with the XCAP-Lite software
150 which results in a total acquisition time of 840 ms. However, the number of frames and
151 therefore the maximum acquisition time can be increased by decreasing the number of
152 pixels to be read out. This allows fields to be recorded that take longer to be delivered
153 than 840 ms, e.g., spread-out Bragg peaks (SOBP). The sensitivity of the sensor can
154 be adjusted by changing between low and high full-well mode, providing an adjustment
155 in dynamic range and sensitivity by a factor of 5.73. The sensor was operated in high
156 full-well mode because of its superior linearity: deviations from a linear response to
157 incoming light is $\pm 0.3\%$ in high full-well mode versus $\pm 2\%$ in low full-well mode. Each
158 pixel has a 14 bit resolution $(16, 384$ counts) and a dark noise floor of $\sim 2,500$ counts.
159 Before taking data, the sensor temperature was given about 15 minutes to stabilise. The
160 remaining temperature dependence shows up as a constant offset along the pixel rows
161 of up to 20 ADC counts. This offset is corrected in data analysis by matching the noise
162 levels in the background image and in the region with no signal of the signal image.
163 The uncertainty on this correction is estimated to be 5 ADC counts.

164 *2.3. Range Telescope*

165 The scintillator sheet stack is held in place by a vice that is screwed to a Thorlabs optical
166 breadboard inside a light-tight enclosure. The proton beam enters the scintillator stack
167 perpendicular to the large face of the scintillator sheets. The enclosure has two entrance
168 windows on either end of the stack, each covered by four layers of aluminium-coated
169 Mylar foil with a WET of ~ 0.03 mm. Light-tight feedthroughs are used for the USB
170 connection and power supply to the CMOS sensor. The CMOS sensor itself is not
171 directly exposed to the beam but is used for the readout of the scintillation light. For
172 this, the image sensor is placed on top of the scintillator stack, fixed by a 3D-printed
173 frame with a second integrated vice. A fibre-optic plate (ISDI) is used to protect the
174 sensor and to couple it to the scintillator. No optical gel is used between the scintillator
175 and image sensor since it was found not to improve the coupling. There is no need
176 for a lens in between the stack and the image sensor due to the segmentation of the
177 scintillator which allows the scintillation light to be attributed to a specific sheet.

178 The resulting range telescope is much more compact than detectors utilising a
179 single monolithic block of scintillator, which normally require a digital camera placed

A scintillator-based range telescope for particle therapy   6

180 up to a metre away from the scintillator to image the entire block [16, 19]. Another
181 advantage of this close-fitting setup is that a larger proportion of the light produced
182 by the scintillator stack is collected and that there are no parallax effects that distort
183 the image. As a consequence, the pixel-to-depth conversion is the same for every pixel
184 such that the whole length of the range telescope can be used without the application
185 of depth-dependent correction factors. Figure 1(a) shows a sketch of the resulting
186 scintillator-based range telescope: a photograph of the resulting experimental setup
187 is shown in figure 1(b).

2.4. Experimental Setup

189 The experiments have been carried out in the experimental room of the Heidelberger
190 Ionenstrahl-Therapiezentrum (HIT, Heidelberg, Germany), except for the radiation
191 hardness assessment, which was performed at the Clatterbridge Cancer Centre (CCC,
192 Bebington, UK). HIT uses a synchrotron to generate treatment beams of protons,
193 helium, carbon or oxygen ions with ranges from 20 to 300 mm. As of January 2020,
194 helium and oxygen ions are not yet available for patient treatment. CCC is a cyclotron-
195 based facility with a fixed beam range of $R_0 = 31.13 \pm 0.20$ mm in water for ocular eye
196 cancer treatment.

197   During the measurements the start of the scintillator stack was always placed in
198 the beam isocentre in order to allow comparison with reference measurements. The
199 detector alignment and positioning was performed using the in-house laser system and
200 a spirit level. Remote control of the computer in the experimental cave was set up to
201 manually trigger the data acquisition when the beam was on. PMMA slabs of known
202 water-equivalent thickness were used to degrade the beam such that the Bragg peak
203 of beams with a larger range than the total detector thickness could be imaged in the
204 scintillator stack. The spill length at HIT was set to 5 s in order to leave enough time
205 for the manual triggering of the image acquisition. The beam intensity at HIT was
206 1.2×10^9 protons per second. At CCC, a brass collimator with a fixed circular opening
207 diameter of 25 mm was used to collimate the double-scattered beam. The dose rate in
208 the Bragg peak at CCC was 2 Gy s^{-1}.

2.5. Generation of a PDL Curve

210 Each proton beam snapshot consists of 21 frames which are averaged in order to
211 compensate for interplay effects between the rolling shutter readout and beam current
212 fluctuations. Background correction is performed by subtracting a background image
213 that was taken with identical measurement conditions but with the beam turned off.
214 Figure 2(a) shows a raw image of a 106.17 MeV proton beam. It can be seen that the
215 sensor has a faulty pixel cluster (white spot, middle left) and a faulty pixel row (white
216 stripe, bottom). These artefacts are corrected for by the background subtraction. The
217 two-dimensional image is then projected onto the beam axis for the generation of a
218 depth-light curve.

A scintillator-based range telescope for particle therapy   7
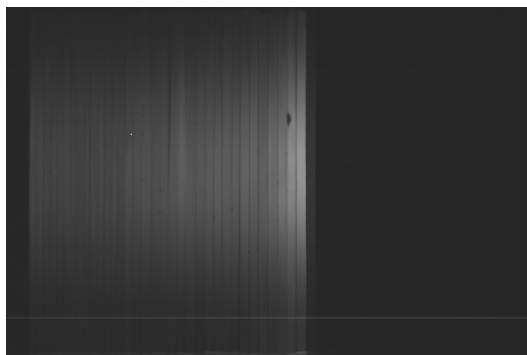
(a) Raw sensor image
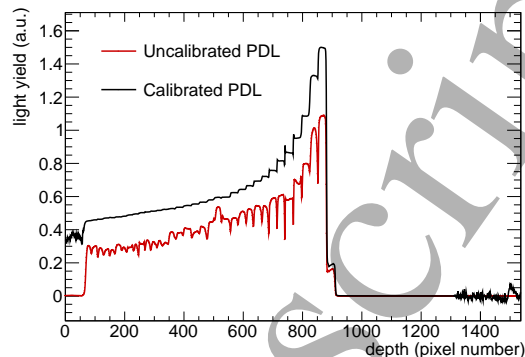
(b) Resulting PDL curve

Figure 2. (a) Raw image of the scintillation light output of a proton beam of 106.17 MeV in the range telescope. The beam travels from left to right. The scintillator starts at a depth of 67 pixels and ends at a depth of 1309 pixels. (b) Background-subtracted and projected PDL of the same measurement as in (a). Calibrated and uncalibrated PDL are shown for comparison.

²¹⁹ In order to calibrate the light output of the scintillator, so-called "shoot-through"
²²⁰ curves are used. A shoot-through (ST) curve is a PDL curve of the highest available
²²¹ proton beam energy (222.71 MeV at HIT) as measured by the range telescope. A
²²² PMMA degrader of 5 cm thickness is placed in front of the stack in order to avoid the
²²³ dose build-up region at the entrance of the Bragg curve [28]. This creates a relatively flat
²²⁴ depth-dose curve in the scintillator stack. The ST measurement is performed from both
²²⁵ sides of the scintillator stack in order to correct for the remaining slope in the Bragg
²²⁶ curve plateau. The resulting averaged ST encodes all information about the coupling
²²⁷ of each individual sheet to the CMOS sensor. A PDL curve is calibrated by performing
²²⁸ a point-by-point division by the averaged ST curve.

²²⁹ A calibrated and an uncalibrated curve, after background subtraction, are shown in
²³⁰ figure 2(b) for comparison. It can be seen that the calibration corrects for the variable
²³¹ coupling of the scintillator sheets and thus yields a smoother PDL curve. The calibration
²³² amplifies the noise in the region where there is no scintillator (pixel numbers 1–66
²³³ and 1310–1536); this is of no importance since these regions do not form part of the
²³⁴ measurement volume and are ignored in further analysis.

²³⁵ The light coupling of the scintillator to the sensor varies along the readout face of
²³⁶ the sheet. It is therefore important to use a shoot-through curve measured at the same
²³⁷ transverse spot position and with the same spot size as the proton pencil beams for the
²³⁸ calibration. The influence of the transverse beam spot position and size on the range
²³⁹ measurement is discussed in section 3.3 and 3.4, respectively.

²⁴⁰ The pixel-to-depth conversion is performed by attributing a depth of zero to the
²⁴¹ pixel row at the start of the scintillator stack and a depth equivalent to the water-
²⁴² equivalent thickness of the whole stack to the last pixel row. The light output in each
²⁴³ sheet is averaged and attributed to the water-equivalent depth at the centre of the

A scintillator-based range telescope for particle therapy 8

respective sheet. During averaging, the light output within 0.5 mm of the edge of a sheet is neglected in order to reduce the influence of crosstalk. The uncertainty on the sheet light output is estimated by taking into account various effects: the beam widening along the path through the material (0.5% of light output), a beam spot size mismatch between the calibration ST and the PDL curve measurement (0.5%), the crosstalk between sheets (0.4% of light output in the neighbouring sheets) as well as sensor temperature differences between measurements (5 ADC counts).

2.6. Quenched Bragg Curve

In order to measure the range of the proton beam, a "quenched Bragg curve" [25] (QB) is fitted to the measured depth-light curve. The quenched Bragg curve is a combination of a model for a percent depth-dose curve by Bortfeld [29] and a model for quenching effects in plastic scintillator by Birks [12]. This model was specifically developed to enable the range reconstruction from PDL curves with low spatial resolution. The QB model provides excellent range reconstruction accuracy of <0.16 mm in the case of a simulated detector with sheets 0.1 mm thick [25]. However, the sheets in the range telescope — and therefore the spatial resolution — are 2–3 mm thick. As such, the quenched Bragg curve is not directly fitted to the depth-light curve but integrated in segments that match the thickness of each sheet: the integrated bins are then used to fit the PDL curves from the range telescope. This method enables a partial compensation of the lower spatial resolution and improves the range fit accuracy to < 0.2 mm.

Table 1 lists the parameters used in the quenched Bragg curve fit. The density ρ is the density of water since the depth was converted to water equivalent depth before fitting. The parameters α, p, β and γ were obtained from Bortfeld's publication [29], which also contains an in-depth explanation of each parameters. For the quenched Bragg fit to the PDL curve, R_0, σ, Φ_0 and kB are used as fit parameters, where σ represents the peak width, Φ_0 stands for the proton fluence and kB is Birks' constant [25]. All remaining model parameters are fixed during the fitting. The quenched Bragg model is implemented using the software toolkit ROOT [30]. Curve fitting is performed with the standard ROOT fit algorithm (Pearson χ^2 test) [31].

The quenched Bragg curve and Bortfeld's Bragg curve model utilise the same parameters. One can therefore use the parameters fitted to the PDL curve as an input for Bortfeld's Bragg curve in order to reconstruct the original depth-dose curve as described in [25].

2.7. Reference PDD Curves at HIT

The reconstructed PDD curve is compared to a reference PDD curve in order to assess the goodness of the reconstruction for the experimental data taken at HIT. These reference PDD curves have been simulated in Fluka [32] and benchmarked against ionisation chamber measurements [33]. An offset of -3.05 ± 0.10 mm is applied to the reference curves to account for the water-equivalent path length (WEPL) from the

A scintillator-based range telescope for particle therapy 9

Table 1. Values of parameters used in the quenched Bragg curve fit. Table adapted from table 1 in [29].

Variable	Description	Value	Unit
p	Exponent of range-energy relation	1.77 [29]	1
α	Proportionality factor	0.022 [29]	mm MeV^{-p}
β	Slope parameter of fluence reduction	0.0012 [29]	mm^{-1}
γ	Fraction of locally absorbed energy	0.6 [29]	1
ρ	Density of water	1.0	g cm^{-3}
S	Scintillation light constant	9 744 [26]	photons MeV^{-1}
R_0	Proton beam range	fit parameter	mm
σ	Width of Gaussian range straggling	fit parameter	mm
Φ_0	Fluence factor	fit parameter	particles mm^{-2}
kB	Birks' constant	fit parameter	mm MeV^{-1}

283 exit of the vacuum chamber to the beam isocentre [34]. The reference range is defined
284 as the 80% distal dose fall-off of a reference PDD curve. The maximum deviation from
285 measured beam ranges is given as 0.2 mm [33], which includes the uncertainty on the
286 WEPL to the isocentre and the reproducibility of the proton beam.

287 3. Results

288 3.1. Proton Range Measurement

289 The quenched Bragg curve described in section 2.6 has been fitted to 32 PDL curves
290 with proton energies ranging from 48.45 MeV to 222.71 MeV. The fit range ends shortly
291 after the Bragg peak since the QB model does not include the dose deposition from
292 neutral particles which dominate beyond the Bragg peak. Figure 3 shows two examples
293 of such a fit for proton beams of 106.17 MeV and 222.71 MeV respectively. The subplots
294 below show the percentage residuals of the QB curve fit. For 222.71 MeV, a total of
295 232.87 mm WET PMMA degrader was placed upstream of the range telescope in order
296 to shift the Bragg peak into the range telescope. The WET of these PMMA degraders
297 was measured with a PTW Peakfinder water column by measuring the range pull-back
298 of a carbon beam which was chosen because of its narrower peak.

299 Alongside the measured PDL curve and resulting quenched Bragg curve fit, the
300 reconstructed PDD curve as well as a reference PDD curve are also plotted. The
301 reconstructed PDD curve is Bortfeld's Bragg curve model plotted with the parameters
302 determined by the QB curve fit. The reference PDD curve is a benchmarked Fluka
303 simulation [33]. The reconstructed PDD curve is normalised such that its peak has the
304 same magnitude as the reference PDD curve. The measured PDL curve is normalised
305 such that its value at zero depth equals the first value of the reference PDD curve.

A scintillator-based range telescope for particle therapy

10

(a) 106.17 MeV
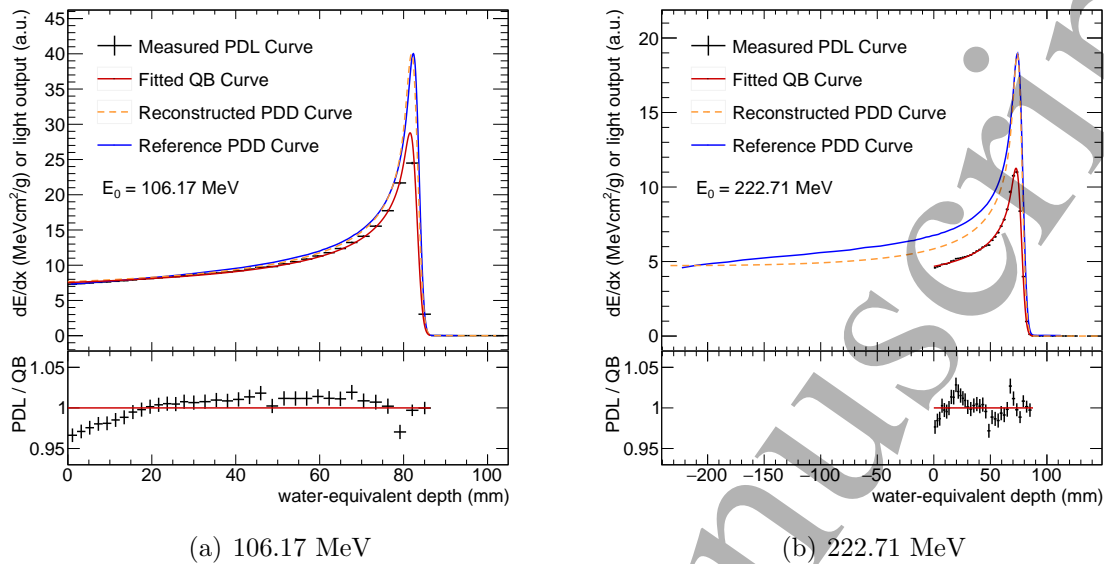
(b) 222.71 MeV

Figure 3. Quenched Bragg curve fit to proton PDL curves and corresponding Bragg curve reconstruction with comparison to reference PDD curves for two beam energies. The 222.71 MeV data includes a PMMA degrader of 232.87 mm WET upstream of the range telescope, hence the missing data.

The quenched Bragg curve describes the measured PDL well for both beam energies: the difference is always smaller than 5%, which can be seen in the percentage residuals of figure 3. This quality of fit was also seen for the other measured ranges (not shown).

Furthermore, the reconstructed PDD curve and the reference PDD curve show good overall agreement (within ±15%). Discrepancies can be seen in the plateau upstream of the Bragg peak and the dose build-up region. These stem from the coarse model of nuclear reactions applied in Bortfeld's analytical description of a Bragg curve [29]. These discrepancies increase with increasing beam energy because the dose contribution of nuclear reactions increases with increasing beam energy [35].

In order to assess the accuracy of the range reconstruction, the reconstructed proton range is compared with the reference proton range: this is defined as the 80% fall-off of the distal edge of the reference proton curve. The uncertainty on the reference ranges is estimated to be 0.2 mm. Figure 4(a) shows the difference ΔR_0 between the measured range and the reference range, plotted versus the reference range. Different shades of gray highlight the use of different thicknesses of PMMA degrader which are given at the top of the plot. The red horizontal line marks the reference range. The error bars represent the uncertainty only on the quenched Bragg model fit. A discussion of other sources of uncertainty can be found in section 4.1.

It can be seen that the range reconstruction accuracy is between 0 mm and −0.41 mm. Steps in the range difference can be seen when new PMMA degraders are introduced in the beam path. ΔR_0 is also seen to monotonically decrease with increasing depth in the scintillator stack (saw tooth pattern in figure 4(a)). This indicates

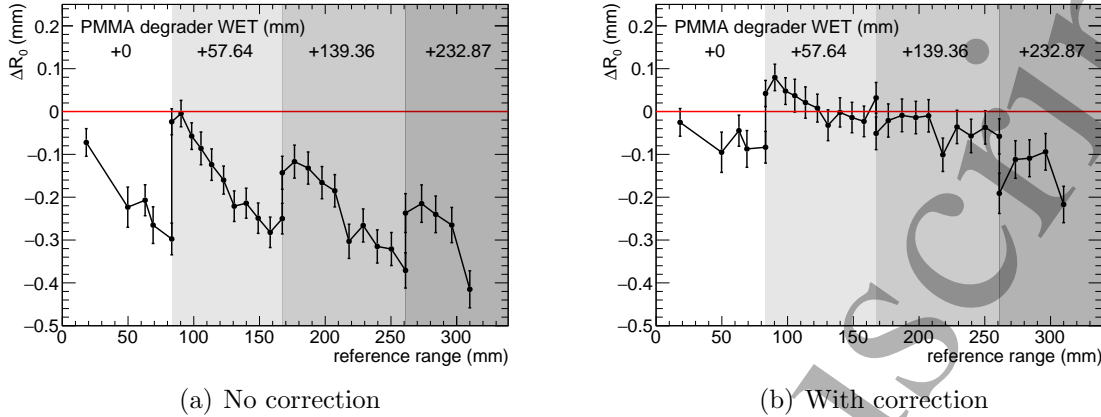*A scintillator-based range telescope for particle therapy*   11

(a) No correction   (b) With correction

Figure 4. Range difference ΔR_0 between the reconstructed proton range and the reference range. The gray sections highlight where different amounts of PMMA degrader have been used. The error bars show only the fit uncertainty. (a) shows the ΔR_0 without any corrections applied. (b) shows the same plot with a corrected scintillator stack WET of 127.6 mm, corresponding to a rotation of $4°$ relative to the beam axis.

a potential underestimation of the actual WET of the scintillator stack. A larger effective WET of the stack could be explained by a small rotation of the stack during measurements i.e. that the stack was not correctly aligned to the beam. Figure 4(b) shows the range difference after the introduction of a rotation of the scintillator stack of $4°$ during the range measurement, resulting in a 0.26% increase in WET. This rotation was performed in post-processing by increasing the value of the stack WET. This correction largely removes the depth-dependence of ΔR_0. The influence of a potential rotation is discussed further in section 4.1.

3.2. Degrader WET

The range pull-back of different PMMA degraders is measured with the range telescope and compared to the range pull-back measured by a PTW Peakfinder. Six PMMA degraders with nominal water-equivalent thicknesses between 1.12 and 59.00 mm are investigated. The displaced air by the degraders is taken into account in the calculation of the WET. The difference between the WETs measured by each method is shown in figure 5 for assumed scintillator stack WETs of 127.27 mm and 127.6 mm, the latter taking into account a potential detector rotation of $4°$ relative to the beam axis. The difference between the measured degrader WET and the reference WET is below 0.1 mm when the stack rotation correction is included.

3.3. Beam Spot Position

A proton beam with an energy of 116.39 MeV was delivered 20 mm to the left and right of the central axis of the scintillator, at the same vertical distance to the CMOS sensor:

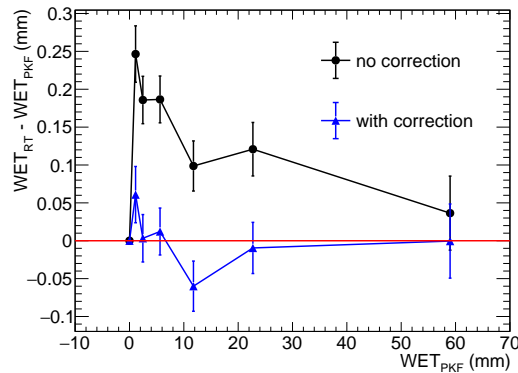*A scintillator-based range telescope for particle therapy*   12

Figure 5. Difference between the PMMA degrader WET measured by the Peakfinder (PKF) and the range telescope (RT): "no correction" refers to the measurement performed with an assumed WET of the scintillator stack of 127.27 mm and "with correction" is for a detector WET of 127.6 mm, corresponding to a rotation of $4°$ relative to the beam axis.
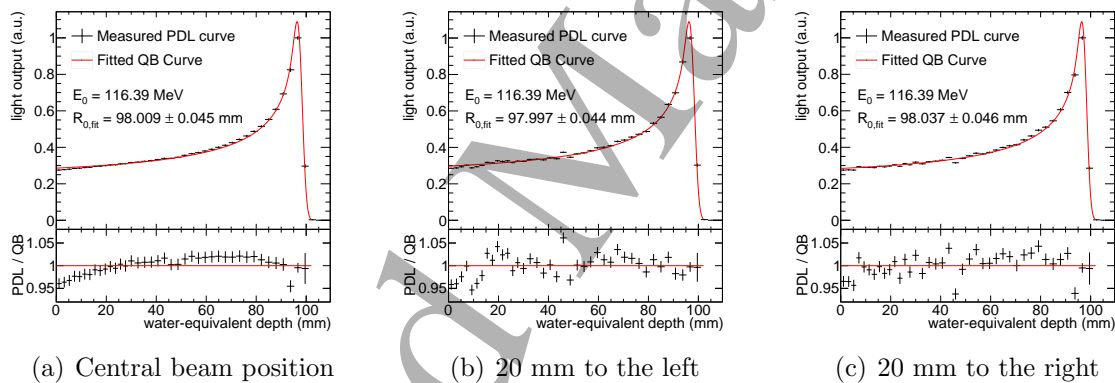
(a) Central beam position   (b) 20 mm to the left   (c) 20 mm to the right

Figure 6. Influence of the beam spot position on the light output. (a) central beam spot, (b) beam spot shifted 20 mm to the left (beam's eye view) and (c) beam spot shifted 20 mm to the right. $R_{0,fit}$ is given with fit uncertainty only.

349 the measured PDL curves are shown in figure 6. The same averaged ST curve is used for
350 the light calibration of the three curves. The different spot position between calibration
351 ST and measurement introduces noise as can be seen by comparing figure 6(a) with 6(b)
352 and 6(c). Variations in the light output in a sheet of up to 7% are observed. These
353 variations could be avoided by repeating the calibration shoot-through measurement at
354 the respective spot position. Another possibility would be to use more reflective material
355 such as Mylar foil for the wrapping of the sheets in order to reduce the transverse
356 position-dependence of the light output. However, the observed variation in range is
357 below 0.04 mm which is within the fit uncertainty on the range measurement. It can be
358 concluded that the beam range measurement is robust against small horizontal offsets
359 from the central axis. Simulations suggest that this is also the case for small vertical
360 beam offsets; however, this was not verified experimentally. The results also set a limit

A scintillator-based range telescope for particle therapy   13

361 to the influence of the non-uniformity in the sheet thickness (± 0.02 mm) on the beam
362 range measurements. Such non-uniformity would show up as a position-dependent beam
363 range, which is shown to be lower than 0.04 mm.
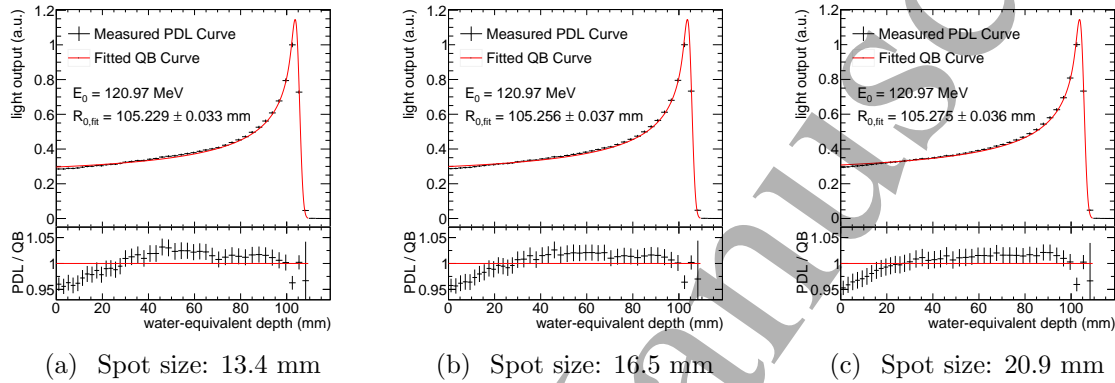
364 *3.4. Beam Spot Size*

(a) Spot size: 13.4 mm   (b) Spot size: 16.5 mm   (c) Spot size: 20.9 mm

Figure 7. Influence of the beam spot size on the light output. (a) Beam spot size of
13.4 mm FWHM, (b) 16.5 mm and (c) 20.9 mm. $R_{0,fit}$ is given with fit uncertainty
only.

365 A proton beam with an energy of 120.97 MeV was delivered to the range telescope
366 with six different spot sizes ranging from 13.4 to 20.9 mm full-width half-maximum
367 (FWHM). The PDL curves for spot sizes of 13.4, 16.5 and 20.9 mm are shown in
368 figure 7. The maximum difference in light output between specific sheets is found to be
369 2%. However, the range reconstruction produces nearly identical results for all different
370 spot sizes with a maximum range difference of <0.05 mm. It is therefore concluded that
371 it is possible to measure the range of a proton pencil beam with the range telescope
372 independent of the beam spot size and without adapting the beam spot size of the
373 calibration ST. The result also shows that the range measurement is robust against the
374 beam widening due to multiple scattering as the protons slow down in the scintillator
375 stack.

376 *3.5. Radiation Hardness*

377 A major disadvantage of plastic scintillator is that it suffers from a reduction in
378 scintillation light output as a result of radiation damage. It is therefore important to
379 investigate the impact of large amounts of absorbed dose on the detector performance.
380 Experiments to determine the radiation hardness of the detector were carried out at the
381 Clatterbridge Cancer Centre using a collimated double-scattered proton beam with a
382 beam energy of 60 MeV and a reference range of (31.13 ± 0.20) mm in water. A total
383 dose of 6,300 Gy was delivered to the range telescope with measurements of the light

A scintillator-based range telescope for particle therapy   14

output taken at regular intervals during the irradiation. The dose per image frame was
≈ 83 mGy.
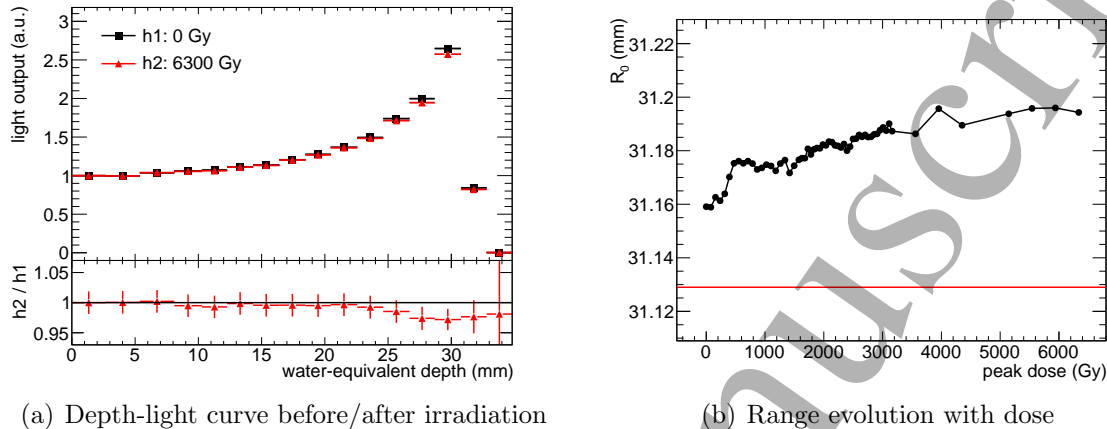
(a) Depth-light curve before/after irradiation   (b) Range evolution with dose

Figure 8. (a) Depth-light curve before and after delivering 6,300 Gy peak dose to the scintillator. (b) Evolution of reconstructed range as a function of the delivered dose at the Bragg peak.

Figure 8(a) shows two measured PDL curves before and after irradiation. The two curves are normalised to the light output in the first sheet because of the fluctuating beam intensity. It can be seen that there is a small reduction of the light output at the Bragg peak of $\sim 3\%$ following the irradiation. Figure 8(b) shows the evolution of the measured range over the course of the radiation hardness assessment. A red horizontal line indicates the value of the reference range. The effect of the peak reduction due to radiation damage can be observed as a small steady increase in the measured beam range. The observed range increase during irradiation is 0.04 mm. The range uncertainty for the Clatterbridge measurements is the same as for the measurement at HIT for a beam range of 31.13 mm (see section 4.1). However, the error bars are not shown in figure 8(b) in order not to overload the plot. The impact of the observed radiation damage is discussed in section 4.2. No radiation damage to the CMOS sensor or the readout electronics was observed.

3.6. Ion Beams

The range telescope was tested with multiple different ion species available at the HIT facility including helium, carbon and oxygen ions. Figure 9 shows four PDL curves of these ions at approximately the same beam range. The curves are normalised to the light output in the first sheet. While the Bragg peak becomes sharper with increasing ion charge, the observed peak-to-plateau ratio in the depth-light curve decreases. This is likely the result of the strong quenching that the ions undergo due to their high specific energy loss as well as the low spatial resolution of the detector which suppresses the tighter peak. As expected, the light production in the fragmentation tail is seen to

A scintillator-based range telescope for particle therapy   15

408 increase with increasing atomic number of the projectile. The range of the ion beams
409 has not been evaluated because of the lack of an analytical description of the ion PDL
410 curve at the present day. The development of an analytical function for the ion beam
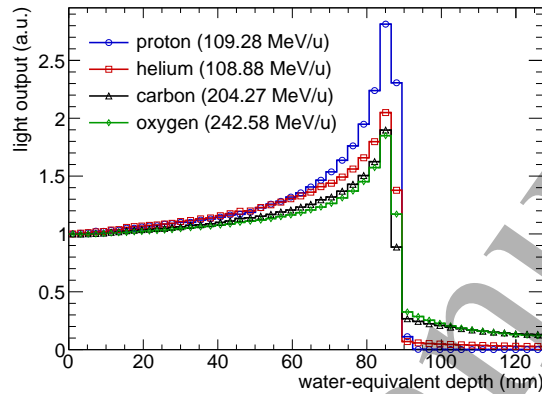411 Bragg curve which includes the projectile fragmentation is part of future work.

Figure 9. Comparison of different ion beams with approximately the same range in the range telescope.

412 **4. Discussion**

413 *4.1. Range Uncertainty*

414 All identified range uncertainty sources are listed and quantified in table 2.

Table 2. Beam range uncertainty sources split up into different beam range sections. (*) is the quadratic sum without misalignment- and degrader-related uncertainties.

	Range uncertainty (mm)			
Beam range (mm)	18–83	83–170	170–260	260–310
Fit uncertainty	0.04	0.04	0.04	0.04
Stopping power ratio	0.05–0.15	0.05–0.15	0.05–0.15	0.05–0.15
QB model	0.2	0.2	0.2	0.2
Calibration ST	0.04–0.16	0.03–0.27	0.04–0.39	0.05–0.14
Stack WET (PKF)	0.01–0.03	0.01–0.03	0.01–0.04	0.01–0.02
Stack WET (rotation)	0.04–0.2	0.06–0.27	0.07–0.30	0.07–0.19
Degrader WET	0	0.04	0.08	0.14
Quadratic sum	0.22–0.36	0.22–0.46	0.24–0.56	0.27–0.37
Quadratic sum*	0.21–0.25	0.21–0.26	0.21–0.26	0.21–0.25

A scintillator-based range telescope for particle therapy   16

₄₁₅ *Degrader WET:* A rotation uncertainty on the placement of the PMMA degraders of
₄₁₆ $2°$ relative to the beam direction is realistic — either during degrader characterisation
₄₁₇ or range measurement — which results in an uncertainty on the degrader WET and
₄₁₈ thus the proton range of up to ± 0.14 mm. This uncertainty is caused by the difficulty
₄₁₉ of aligning a small piece of PMMA perpendicular to the laser positioning system and
₄₂₀ the uncertainty of the laser system itself.

₄₂₁ *Stack WET (PKF):* The uncertainty associated with the measurement of the
₄₂₂ scintillator stack WET with the Peakfinder is ± 0.04 mm. This uncertainty was
₄₂₃ determined by repeating the measurement of the range pull-back. It translates into
₄₂₄ a range uncertainty of ± 0.01–0.04 mm.

₄₂₅ *Stack WET (rotation)* A rotation of the scintillator stack of up to $4°$ relative to the
₄₂₆ beam axis during the measurement of PDL curves is realistic, which amounts to a stack
₄₂₇ WET uncertainty of ± 0.3 mm. This translates into a range uncertainty of ± 0.04–
₄₂₈ 0.3 mm, depending on the depth of the proton beam in the scintillator. The uncertainty
₄₂₉ is larger than the one for the PMMA degrader alignment because it is not the scintillator
₄₃₀ stack itself but the light-tight enclosure that is aligned with the laser system. Figure 4(b)
₄₃₁ shows the range difference when the scintillator stack is rotated by $4°$ relative to the
₄₃₂ beam axis. It can be seen that the negative slope in each section of the plot becomes
₄₃₃ more flat and the steps in the range due to the uncertainty on the degrader WET are
₄₃₄ easier to identify. This is a hint that the scintillator stack was indeed misaligned with
₄₃₅ the beam direction by a rotation of approximately $4°$ during the range measurement.

₄₃₆ *Calibration ST:* A potential rotational misalignment of the scintillator stack during
₄₃₇ the shoot-through measurement would result in a depth-dependent distance between
₄₃₈ CMOS sensor and the central beam axis, leading to an averaged ST curve that has a
₄₃₉ systematic error. When the light calibration is performed with an averaged ST curve
₄₄₀ that has a rotational misalignment, an artificial slope would be introduced into the PDL
₄₄₁ curve. The effect on the light output of a stack rotation of $4°$ is estimated by the means
₄₄₂ of a Geant4 [36, 37, 38] simulation. The QB model is then fitted to the PDL curve
₄₄₃ with and without the simulated correction in order to determine the effect on the range
₄₄₄ reconstruction. The effect on the range measurement is found to be ± 0.03–0.39 mm.

₄₄₅ *Quenched Bragg model:* The QB model was shown in simulation to always reproduce
₄₄₆ the reference proton range within 0.2 mm for proton beam energies between 60–240 MeV
₄₄₇ and a spatial resolution of 3 mm. This systematic deviation can be explained by the lack
₄₄₈ of an appropriate description of nuclear reactions in Bortfeld's Bragg curve model [29].

₄₄₉ *Stopping power ratio:* The water-equivalent thickness of the scintillator depends on
₄₅₀ the beam energy with which it is probed due to the variation in stopping power ratio
₄₅₁ (SPR) of water and polystyrene. This effect is quantified using the SPR data for water

A scintillator-based range telescope for particle therapy   17

452 and polystyrene availaible from the NIST database [39]. The effect on the proton range
453 was found to be ±0.05–0.15 mm, depending on the depth of the proton beam in the
454 scintillator stack.

455 *Fit uncertainty:* The uncertainty on the fitted range parameter, R_0 that is returned by
456 the minimisation process is approximately ±0.04 mm, independent of the beam range.
457 Its value depends on the uncertainty of the light output in each scintillator sheet.

458 The dominant range uncertainties mentioned above are caused not by the range
459 telescope detection technique itself but either by poor detector alignment (rotation
460 uncertainty) or the use of PMMA degraders. Range uncertainties inherent to the range
461 telescope are the fit uncertainty, the QB model uncertainty and the stopping power
462 ratio. If the external range uncertainties are reduced — e.g., by improving the detector
463 alignment or by avoiding the use of PMMA degraders — the range uncertainty could be
464 reduced to approximately ±0.26 mm (see bottom line in table 2). One of the dominant
465 range uncertainties would then be the stopping power ratio which could be corrected
466 for using the SPR tables in the NIST database.

467 *4.2. Radiation Damage*

468 The radiation damage measurements described in Section 3.5 show that 6,300 Gy of
469 integrated dose leads to a relative reduction of the light output of 3% at the Bragg peak
470 compared to the entrance. The resulting impact on the range reconstruction is found to
471 be 0.04 mm at a range in water of 31.13 mm: this is well within the uncertainty on the
472 range measurement presented above (±0.21 mm) and the reference range (±0.2 mm).
473 At an assumed entrance dose rate of 0.25 Gy s^{-1} (the typical clinical entrance dose rate
474 at Clatterbridge Cancer Centre) a beam spot measurement with a typical duration of
475 10 ms [40] would deliver an entrance dose of 0.0025 Gy to the detector. In order to see a
476 scintillator damage comparable to the one in figure 8(a) after delivering 6,300 Gy peak
477 dose, about $500,000$ beam measurements would need to be performed (peak-to-entrance
478 dose ratio of 4.7 at CCC). Furthermore, the light output of the detector can easily be
479 recalibrated following the procedure described in section 2.5 which would correct for
480 any radiation damage. The detector is therefore believed to be able to deliver long-term
481 reliable range measurements at clinical proton dose rates.

482 *4.3. Comparison With Other Range Detectors*

483 The main disadvantages of the scintillator-based range telescope are the radiation
484 damage, the low spatial resolution and the sensitivity to misalignment. The first two
485 are found to be manageable by occasional re-calibration and the use of a bespoke range
486 reconstruction algorithm. An updated prototype detector will require a positioning
487 system that reduces the detector alignment uncertainty to below 2°.

A scintillator-based range telescope for particle therapy   18

A major advantage of the scintillator is that it has a density similar to that of water which facilitates the direct measurement of water-equivalent depth compared with multi-layer ionisation chambers. The detector does not require high voltage for operation and unlike ionisation chambers its light output is independent of the dose rate. This is important for high dose-per-pulse beams (FLASH proton therapy) for which ionisation chambers have been shown to have a dramatically reduced ion collection efficiency [41].

Thanks to the absence of a lens, no depth-dependent correction factors need to be applied to the measured light output as is the case for monolithic scintillation detectors with a single camera. The compact and lightweight design would enable the detector to be mounted to the beam nozzle such that one could easily perform range measurements at different gantry angles.

It is of note that the quenched Bragg curve utilised for fitting does not require simulations of the LET distribution in the scintillator in order to correct for the light quenching. Instead, both the LET distribution and the quenching correction are fitted simultaneously, thus avoiding a potential mismatch between the two. The range reconstruction uncertainty without PMMA degraders and with improved detector alignment would be on the order of ± 0.26 mm. Comparable commercial detectors such as the IBA Giraffe have a range reconstruction uncertainty of 0.5 mm[8]. Furthermore, the range telescope is shown to be able to cope with proton beams of different spot sizes as well as off-axis beams which is important if scanned beams shall be measured without moving the detector.

4.4. Applications in Particle Therapy

Initially, the detector was designed to perform range quality assurance measurements of proton pencil beams. However, the detector is also suitable for measuring the WET of any beam degrader material, immobilisation devices or samples of implants that can be found in the beam path. Furthermore, it could be used as the range measurement stage in a patient-specific QA detector. For this, the light readout would need to be faster in order to allow the measurement of single beam spots. Routes towards faster light readout are discussed in section 4.5.

In addition, the range telescope could be used for the measurement of the residual range of a beam that passes through a patient, either using patient range probing [42] or in a potential mixed helium/carbon beam [18, 43]. This would enable the detection of inter- or intra-fractional movements of the tumour: for further discussion see [43].

There is also the potential of using the range telescope for range QA measurements of ion beams. However, more work would need to go into the development of a quenched Bragg curve model for ion beams that also takes into account dose deposition from beam fragmentation in order to achieve a clinically relevant range reconstruction accuracy.

A scintillator-based range telescope for particle therapy 19

4.5. Future Work

A large range uncertainty is currently the use of PMMA degraders, which were necessary with the existing setup to measure the full range of clinical particle beam energies due to the limited WET of the scintillator stack. Furthermore, the large-scale CMOS sensor offers a two-dimensional resolution that is not necessary for range measurements whilst being fragile and delicate to handle. Future work will therefore focus on developing a full-scale range telescope (WET ≈ 30 cm) with a custom light-detection system based on photodiodes. In this new setup, each scintillator sheet will be coupled to a single photodiode. Custom-built readout electronics will allow the range telescope readout to be synchronised with the beam delivery for an automated data acquisition. This new system will also be faster than the current light readout and therefore allow the measurement of individual beam spots that take on the order of milliseconds to be delivered.

A potential upgrade of the detector with another system for making 2D beam spot and position measurements upstream of the scintillator stack for quasi-3D beam measurements is also being considered.

5. Conclusion

A novel range telescope based on plastic scintillator sheets and a CMOS image sensor readout has been developed and tested with clinical proton beams. The proposed design avoids optical artefacts that are common in scintillation detectors. The maximum range difference between measurement and reference is -0.41 mm at a beam range of 310 mm. The difference is smaller if no PMMA degraders are used and a potential rotation of the detector during the measurements is taken into account. The water-equivalent thickness of different PMMA degraders is reconstructed within ± 0.1 mm in range pull-back measurements. This accuracy is achieved with a bespoke image analysis and range reconstruction algorithm that simultaneously fits the LET distribution and the quenching correction along the proton path in the scintillator. A radiation hardness evaluation demonstrates that the scintillator has the capability to fulfil the longevity requirements in a clinical proton therapy centre by showing only 3% light output reduction following a dose deposition worth about $500,000$ beam spot measurements, with a change in measured range well within the uncertainty of the detector range measurement. The range reconstruction accuracy is also insensitive to small changes in the beam spot size, the lateral beam position within the detector and the initial particle energy. Range measurements of ion beams are also possible but require the development of a new depth-light curve model in order to achieve a similar range reconstruction accuracy compared with protons.

A scintillator-based range telescope for particle therapy   20

Acknowledgments

References

[1] Particle Therapy Co-Operative Group. Particle therapy facilities in clinical operation. https://www.ptcog.ch/index.php/facilities-in-operation, June 2019. Accessed on 2019-08-07.

[2] I. Kristensen, K. Nilsson, and P. Nilsson. Comparative Proton and Photon Treatment Planning in Pediatric Patients with Various Diagnoses. *Internaltional Journal of Particle Therapy*, 2015.

[3] M. T. Gillin, N. Sahoo, M. Bues, G. Ciangaru, G. Sawakuchi, F. Poenisch, B. Arjomandy, C. Martin, U. Titt, K. Suzuki, A. R. Smith, and X. R. Zhu. Commissioning of the discrete spot scanning proton beam delivery system at the University of Texas M.D. Anderson Cancer Center, Proton Therapy Center, Houston. *Medical Physics,* 37(1):154–163, 2010.

[4] L. Grevillot, M. Stock, H. Palmans, J. Osorio Moreno, V. Letellier, R. Dreindl, A. Elia, H. Fuchs, A. Carlino, and S. Vatnitsky. Implementation of dosimetry equipment and phantoms at the MedAustron light ion beam therapy facility. *Medical Physics*, 45(1):352–369, 2018.

[5] O. Actis, D. Meer, S. Koenig, D.C. Weber, and A. Mayor. A comprehensive and efficient daily quality assurance for PBS proton therapy. *Physics in Medicine and Biology*, 62(5), March 2017.

[6] S. Rana, J. Bennouna, E. J. J. Samuel, and A. N. Gutierrez. Development and long-term stability of a comprehensive daily QA program for a modern pencil beam scanning (PBS) proton therapy delivery system. *Journal of Applied Clinical Medical Physics*, 20(4):29–44, 2019.

[7] C. P. Karger, O. Jäkel, H. Palmans, and T. Kanai. Dosimetry for ion beam radiotherapy. *Physics in Medicine and Biology*, 55, 2010.

[8] C. Baeumer, B. Koska, J. Lambert, B. Timmermann, T. Mertens, and P. T. Talla. Evaluation of detectors for acquisition of pristine depth-dose curves in pencil beam scanning. *Journal of Applied Clinical Medical Physics*, 16(6):151–163, 2015.

[9] L. Karsch, E. Beyreuther, T. Burris-Mog, S. Kraft, C. Richter, K. Zeil, and J. Pawelke. Dose rate dependence for different dosimeters and detectors: TLD, OSL, EBT films, and diamond detectors. *Medical Physics*, 39(5):2447–2455, 2012.

[10] L. Beaulieu and S. Beddar. Review of plastic and liquid scintillation dosimetry for photon, electron, and proton therapy. *Physics in Medicine and Biology*, 61, 2016.

[11] G. F. Knoll. *Radiation Detection and Measurement.* Wiley, 1979.

[12] J. B. Birks. Scintillations from Organic Crystals: Specific Fluorescence and Relative Response to Different Radiations. *Proceedings of the Physical Society A*, 64:874, 1951.

[13] S Russo, A Mirandola, S Molinelli, E Mastella, A Vai, G Magro, A Mairani, D Boi, M Donetti, and M Ciocca. Characterization of a commercial scintillation detector for 2-D dosimetry in scanned proton and carbon ion beams. *Physica Medica*, 34, 2017.

[14] S. N. Boon, P. van Luijk, J. M. Schippers, H. Meertens, J. M. Denis, S. Vynckier, J. Medin, and E. Grusell. Fast 2D phantom dosimetry for scanning proton beams. *Medical Physics*, 25(4):464–475, 1998.

[15] C. Hoehr, C. Lindsay, J. Beaudry, C. Penner, V. Strgar, R. Lee, and C. Duzenli. Characterization of the exradin W1 plastic scintillation detector for small field applications in proton therapy. *Physics in Medicine and Biology*, 63, 2018.

A scintillator-based range telescope for particle therapy 21

[16] Y. Fukushima, M. Hamada, T. Nishio, and K. Maruyama. Development of an easy-to-handle range measurement tool using a plastic scintillator for proton beam therapy. *Physics in Medicine and Biology*, 51, 2006.

[17] M. Almurayshid, Y. Helo, A. Kacperek, J. Griffiths, J. Hebden, and A. Gibson. Quality assurance in proton beam therapy using a plastic scintillator and a commercially available digital camera. *Journal of applied cinical medical physics*, 2017.

[18] D. Mazzucconi, S. Agosteo, M. Ferrarini, L. Fontana, V. Lante, M. Pullia, and S. Savazzi. Mixed particle beam for simultaneous treatment and online range verification in carbon ion therapy: Proof-of-concept study. *Medical Physics*, 42, 2018.

[19] S. Beddar, L. Archambault, N. Sahoo, F. Poenisch, G. T. Chen, M. T. Gillin, and R. Mohan. Exploration of the potential of liquid scintillators for real-time 3d dosimetry of intensity modulated proton beams. *Medical Physics*, 36(5):1736–1743, 2009.

[20] L. Archambault, F. Poenisch, N. Sahoo, D. Robertson, A. Lee, M. T. Gillin, R. Mohan, and S. Beddar. Verification of proton range, position, and intensity in impt with a 3d liquid scintillator detector system. *Medical Physics*, 39(3):1239–1246, 2012.

[21] C. D. Darne, F. Alsanea, D. G. Robertson, N. Sahoo, and S. Beddar. Performance characterization of a 3D liquid scintillation detector for discrete spot scanning proton beam systems. *Physics in Medicine and Biology*, 62, 2018.

[22] D. Robertson, C.K. Hui, L. Archambault, R. Mohan, and S. Beddar. Optical artefact characterization and correction in volumetric scintillation dosimetry. *Physics in Medicine and Biology*, 59, 2014.

[23] D. Robertson, D. Mirkovic, N. Sahoo, and S. Beddar. Quenching correction for volumetric scintillation dosimetry of proton beams. *Physics in Medicine and Biology*, 58, 2013.

[24] F. Alsanea, C. Darne, D. Robertson, and S. Beddar. Ionization quenching correction for a 3D scintillator detector exposed to scanning proton beams. *Physics in Medicine and Biology*, 65(7):075005, April 2020.

[25] L. Kelleter and S. Jolly. A mathematical expression for depth-light curves of therapeutic proton beams in a quenching scintillator. *Medical Physics*, 2020.

[26] NuviaTech Instruments. *NuDET Plastic: Specification Sheet*, October 2019.

[27] H.N. Subrahmanyam and S.V. Subramanyam. Thermal expansion of irradiated polystyrene. *Journal of Materials Science*, 22, 1987.

[28] L. Kelleter, B. Zhen Hong Tham, R. Saakyan, J. Griffiths, R. Amos, S. Jolly, and A. Gibson. Technical Note: Simulation of dose buildup in proton pencil beams. *Medical Physics*, 2019.

[29] T. Bortfeld. An analytical approximation of the Bragg curve for therapeutic proton beams. *Medical Physics*, 24, 1997.

[30] R. Brun and F. Rademakers. ROOT: An object oriented data analysis framework. *Nuclear Instruments and Methods*, A389:81–86, 1997.

[31] R. Brun and F. Rademakers. ROOT User's Guide 6. https://root.cern.ch/root/htmldoc/guides/users-guide/ROOTUsersGuide.html, May 2018. Accessed on 2019-11-21.

[32] G. Battistoni, J. Bauer, T. T. Boehlen, F. Cerutti, M. P. W. Chin, R. Dos Santos Augusto, A. Ferrari, P. G. Ortega, W. Kozłowska, G. Magro, A. Mairani, K. Parodi, P. R. Sala, P. Schoofs, T. Tessonnier, and V. Vlachoudis. The FLUKA Code: An Accurate Simulation Tool for Particle Therapy. *Frontiers in Oncology*, 6:116, 2016.

[33] K. Parodi, A. Mairani, S. Brons, B. G. Hasch, F. Sommerer, J. Naumann, O. Jäkel, T. Haberer, and J. Debus. Monte Carlo simulations to support start-up and treatment planning of scanned proton and carbon ion therapy at a synchrotron-based facility. *Physics in Medicine and Biology*, 57, 2012.

[34] P. Heeg. Private communication. 2019-12-02.

[35] W.D. Newhauser and R. Zhang. The physics of proton therapy. *Physics in Medicine and Biology*, 60, 2015.

A scintillator-based range telescope for particle therapy 22

[36] S. Agostinelli et al. Geant4: A Simulation toolkit. *Nuclear Instruments and Methods*, A506:250–303, 2003.

[37] J. Allison et al. Geant4 developments and applications. *IEEE Transactions on Nuclear Science*, 53(1):270–278, Feb 2006.

[38] J. Allison et al. Recent developments in Geant4. *Nuclear Instruments and Methods in Physics Research Section A: Accelerators, Spectrometers, Detectors and Associated Equipment*, 835:186 – 225, 2016.

[39] M. J. Berger, J. S. Coursey, M. A. Zucker, and J. Chang. Stopping-Power and Range Tables for Electrons, Protons, and Helium Ions. *NIST Standard Reference Database 124*, 2017.

[40] S. van de Water, H. M. Kooy, B. J. M. Heijmen, and M. S. Hoogeman. Shortening Delivery Times of Intensity Modulated Proton Therapy by Reducing Proton Energy Layers During Treatment Plan Optimization. *International Journal of Radiation Oncology*Biology*Physics*, 92(2):460 – 468, 2015.

[41] K. Petersson, M. Jaccard, J.-F. Germond, T. Buchillier, F. Bochud, J. Bourhis, M.-C. Vozenin, and C. Bailat. High dose-per-pulse electron beam dosimetry - a model to correct for the ion recombination in the advanced markus ionization chamber. *Medical Physics*, 44(3):1157–1167, 2017.

[42] M. Mumot, C. Algranati, M. Hartmann, J. M. Schippers, E. Hug, and A. J. Lomax. Proton range verification using a range probe: definition of concept and initial analysis. *Physics in Medicine and Biology*, 55(16):4771–82, 2010.

[43] L. Volz, L. Kelleter, S. Brons, L. N. Burigo, C. Graeff, N. I. Niebuhr, R. Radogna, S. Scheloske, C. Schoemers, S. Jolly, and J. Seco. Experimental exploration of a mixed helium/carbon beam for online treatment monitoring in carbon ion beam therapy. *Physics in Medicine and Biology*, 2020.